

Experimental realization of supergrowing fields

Sethuraj K. R.^{1,2,*}, Tathagata Karmakar^{3,2,4,†}, S. A. Wadood^{1,2,5},

Andrew N. Jordan^{4,3,2}, and A. Nick Vamivakas^{1,2,3,6‡}

¹The Institute of Optics, University of Rochester, Rochester, NY 14627, USA

²Center for Coherence and Quantum Optics, University of Rochester, Rochester, NY 14627, USA

³Department of Physics and Astronomy, University of Rochester, Rochester, NY 14627, USA

⁴Institute for Quantum Studies, Chapman University, Orange, CA 92866, USA

⁵Currently with Department of Electrical Engineering, Princeton University, NJ, 08544, USA and

⁶Materials Science, University of Rochester, Rochester, NY 14627, USA

(Dated: September 4, 2023)

Supergrowth refers to the local amplitude growth rate of a signal being faster than its fastest Fourier mode. In contrast, superoscillation pertains to the variation of the phase. Compared to the latter, supergrowth can have exponentially higher intensities and promises improvement over superoscillation-based superresolution imaging. Here, we demonstrate the experimental synthesis of controlled supergrowing fields with a maximum growth rate of ~ 19.1 times the system-bandlimit. Our work is an essential step toward realizing supergrowth-based far-field superresolution imaging.

Superresolution in optical imaging refers to approaches that can boost spatial resolution beyond the diffraction limit of light. The diffraction limit defines the smallest feature size that can be resolved in a standard optical imaging system and is determined by the light's wavelength and the optical system's numerical aperture (NA) [1]. One way to resolve subwavelength features in far-field imaging is by using superoscillatory optical spots, a phenomenon where complex fields can locally oscillate at a rate greater than their cut-off spatial frequency [2–6]. Nonetheless, superoscillations have the inherent disadvantage of very small intensity combined with substantial side lobes, leading to poor imaging quality. Both numerical optimization schemes [7] and sophisticated optical setups [8–10] have been investigated for the mitigation of sidelobe intensity. However, supergrowth [11], a recently introduced physical concept, offers a promising route to solve this issue.

In supergrowing fields, the local amplitude growth rate of a complex field is higher than the highest spatial frequency in its Fourier spectrum, thereby also providing access to subwavelength features [12]. This concept has parallels to near-field microscopy with evanescent waves [13, 14]. Supergrowing optical field spots can contain exponentially more intensity compared to superoscillating regions and have been shown theoretically to be able to image subwavelength objects [15]. Moreover, theoretical frameworks for systemic generation of both supergrowing/superoscillating fields have been studied [16]. Currently, supergrowth exists as a purely theoretical construct and has not been realized experimentally.

In this work, we achieve a critical step toward the goal of superresolution using supergrowth, i.e., the synthesis and characterization of supergrowing fields in the laboratory. To accomplish this objective, we elucidate the concept of supergrowth in a diffraction-limited system and identify the critical constraints that can limit supergrowth in an experiment. We also furnish comprehen-

sive methods and tools to quantify supergrowth in any experimental setup effectively. The experimental demonstration lays the foundation for generating supergrowing fields that can be utilized for superresolution imaging.

Supergrowing strength.— The local growth rate $\kappa(x)$ [local wave number $k(x)$] of a bandlimited complex-field $f(x)$ is defined as $\kappa(x) + ik(x) = \partial_x \log [f(x)]$ [12]. The field has supergrowth (superoscillation) at $x = x_0$ when $|\kappa(x_0)| \geq k_{\max}^f$ ($|k(x_0)| \geq k_{\max}^f$), where k_{\max}^f denotes the highest wavenumber of the field. To characterize the amount of supergrowth, we define the supergrowing strength $\Gamma(x) = \left| \frac{\kappa(x)}{k_{\max}^f} \right|$; $f(x)$ is supergrowing at $x = x_0$ when $\Gamma(x_0) \geq 1$.

The intensity associated with field $f(x)$ is $I(x) = |f(x)|^2$, and has a bandlimit of $2k_{\max}^f$. The local growth rate of the intensity $\kappa_I(x)$ is twice that of the original field. The supergrowing strength $\Gamma(x)$ can be obtained from the intensity as

$$\Gamma(x) = \left| \frac{\kappa_I(x)}{2k_{\max}^f} \right|. \quad (1)$$

Equation. (1) has significant implications in the experiment, as we need only transverse intensity information, which can be obtained using a CCD camera. For field-based experimental characterization of growth rate, one needs full-field reconstruction involving more complicated interferometry.

Supergrowth in a diffraction-limited optical system.— The wavelength of illumination λ and an optical system's NA define its diffraction-limited response and maximum spatial frequency ($k_{\max}^s \approx \frac{2\pi}{\lambda} \text{NA}$) that can pass through the system [1]. The bandlimit of the optical system might be different from the field bandlimit k_{\max}^f , although the latter must be upper bounded by the former (i.e. $k_{\max}^f \leq k_{\max}^s$). We note that superresolution imaging using superoscillation/supergrowth is only possible when the local wavenumber/growth rate of the illumination field is higher than the bandlimit of the system

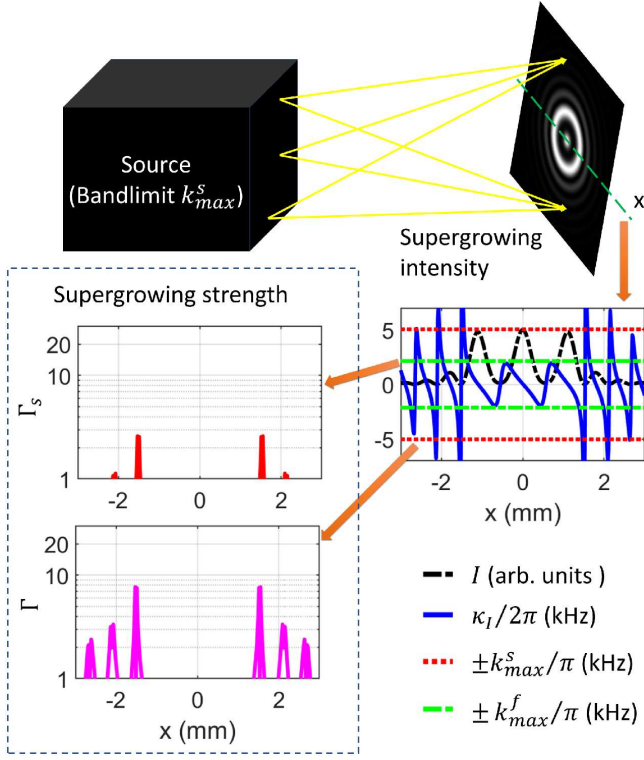


FIG. 1. Conceptual illustration of the dependence of supergrowing on field and system bandlimits. The optical source (shown as a black box) of bandlimit k_{max}^s synthesizes a supergrowing complex field (of bandlimit k_{max}^f) at the image plane. Horizontal line-cut of intensity $I(x)$, and supergrowing strength parameters $\Gamma(x)$ from Eq. (1) and $\Gamma_s(x)$ from Eq. (2) are plotted for a sample function. Since $k_{max}^s \geq k_{max}^f$ in any diffraction-limited optical system, the condition $\Gamma_s \geq 1$ is more restrictive in comparison to $\Gamma \geq 1$. This fact is manifested in the plot since a smaller region is identified by $\Gamma_s \geq 1$.

k_{max}^s . For $k_{max}^f \leq |k|, |\kappa| < k_{max}^s$, superresolution cannot be achieved.

For supergrowing in experiments, the appropriate definition is $|\kappa(x)| \geq k_{max}^s$, so that the benefit of supergrowing can outperform the diffraction-limited performance of an optical system. The supergrowing strength of an optical field in an experiment is

$$\Gamma_s(x) = \left| \frac{\kappa_I(x)}{2k_{max}^s} \right|, \quad (2)$$

where the subscript s in Γ_s indicates that it is defined with respect to the bandlimit of the system. According to this definition, the field $f(x)$ is supergrowing when $\Gamma_s \geq 1$. The optical fields realized in our experiment are supergrowing with respect to both definitions. For convenience, we define the bandlimit ratio $b = (k_{max}^f)/(k_{max}^s)$, such that $\Gamma_s = b \Gamma$.

Figure 1 provides an example of an optical field with different $\Gamma_s(x)$ and $\Gamma(x)$. One can observe that at some points $x = x_0$, the optical field is supergrowing in a mathematical sense ($\Gamma \geq 1$), but not supergrowing ($\Gamma_s < 1$)

based on the definition we use. From here onwards, we stick to the definition of supergrowing strength as Γ_s .

Experiment.—The schematic of the optical setup used to generate supergrowing optical fields is shown in Fig. 2. An intensity-stabilized 795 nm linearly polarized collimated laser beam (Toptica TA 100) passes through a beam expander using lenses L_1 and L_2 . This beam is transferred to a computer-generated phase-only pixelated hologram (CGPPH) generated using a liquid-crystal-based SLM (Hamamatsu LCOS). A beam expander using the lenses L_1 and L_2 ensures the laser beam overfills the active area of the SLM. As a result, the CGPPH sees less spatial variation of intensity of the illuminating laser and a nearly uniform phase. To stabilize the laser intensity, an acousto-optic modulator with a PID controller is used, and polarization optics and attenuators are used to control the polarization and intensity of the laser beam (not shown in the schematic). The diffraction from the CGPPH is Fourier processed using a classical $4f$ processor consisting of lenses L_3 and L_4 , and a precision pinhole P (Thorlabs P1000K). The intensity distribution of the complex field at the image plane (Z_I) is measured using a CCD camera. We have ensured the output intensity lies within the linear response of the detector.

Phase and amplitude of the optical field at co-ordinates (u, v) in the transverse plane Z_F determine the phase and amplitude of image plane (Z_I) Fourier components at $f_x = \frac{u}{\lambda f}$ and $f_y = \frac{v}{\lambda f}$ [1]. The maximum spatial

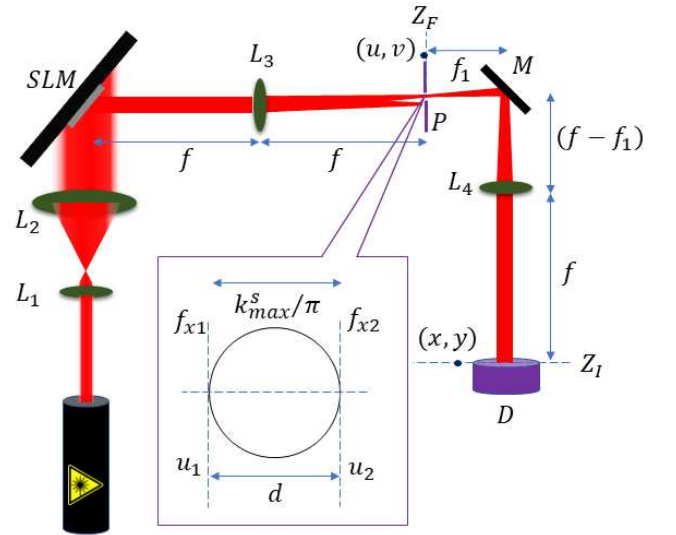


FIG. 2. Optical setup schematic. Notations: L , lens; SLM , Spatial light modulator; f , focal length of lens; Z_F , transverse back focal plane of L_3 ; P , precision pinhole; M , mirror; D , CCD camera; Z_I , image plane; (u, v) , Cartesian coordinates representing any point on the plane Z_F ; (x, y) , Cartesian coordinates representing any point on the plane Z_I ; d , diameter of P ; and f_{x1} and f_{x2} , are horizontal (x) Fourier coordinate of Z_I . The inset shows an expanded view of the transverse cross-section of P .

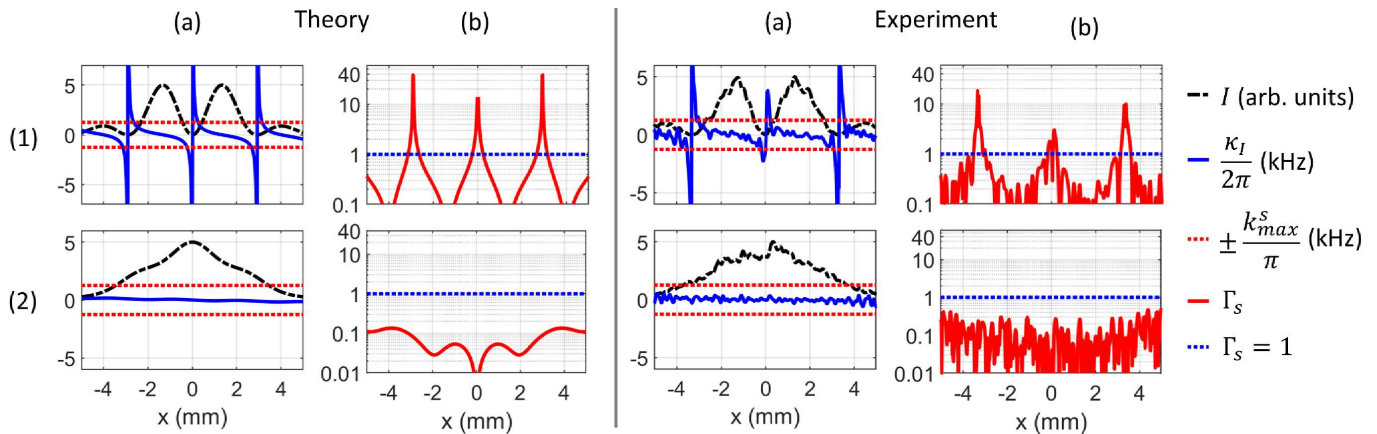


FIG. 3. Simulations [two left columns] and experimental construction [two right columns] of optical fields with [row (1)] and without [row (2)] supergrowth. Columns (a) show x-line-cut of I and κ_I , along with $2k_{\max}^s$, identifying the supergrowing regions. Columns (b) show the x-line-cut of Γ_s from Eq. (2). In (b), the dotted blue line separates the supergrowing region ($\Gamma_s(x) \geq 1$) and non-supergrowing region ($\Gamma_s(x) < 1$). We are able to achieve a maximum supergrowth of $\Gamma_s \approx 18.3$ in the experiment. These plots demonstrate our ability to generate and control supergrowth in an experiment.

frequency at the image plane is limited by the diameter d of the precision pinhole at Z_F , and the system bandlimit is $k_{\max}^s = \frac{\pi d}{\lambda f}$.

Generation of supergrowing functions.— The CGPPH used in the experiment for generating a supergrowing function uses encoding techniques described in [17]. The function to be prepared in the experiment must satisfy two criteria.

1. Bandlimit: $k_{\max}^f < k_{\max}^s$.
2. Spatial-limit: The distribution of supergrowing field at the image plane Z_I must remain within the image of SLM active area at Z_I .

It is a challenge to satisfy both of these criteria as limitations imposed in the spatial domain demand a scaling up in the frequency domain. Larger values of k_{\max}^f are necessary to ensure maximum supergrowth $\Gamma_s \geq 1$ within the spatial limit. Theoretically, $k_{\max}^f = k_{\max}^s$ is possible, but due to experimental imperfection and uncertainties, one cannot achieve this upper limit for a field in experiments.

We explore two different ways of constructing candidate supergrowing functions in a circularly symmetric geometry: 1) heuristic analytical method and 2) numerical simulations. In the first approach, we start with a simple circularly symmetric analytical function with supergrowing features $f(\rho) = f_1(\rho)f_2(\rho)$, where $\rho^2 = x^2 + y^2$. Here, $f_1(\rho) = \exp(\frac{-\rho^2}{2c^2})$, where c is a constant, ensures a limited spatial area extent of $f(\rho)$; and $f_2(\rho) = \cos(k_{f_2}[\rho - \rho_0]) + ia \sin(k_{f_2}[\rho - \rho_0])$, where the shift ρ_0 is such that the maximum or minimum of $|f_2(\rho)|$ is at $\rho = 0$. Also, a is a parameter much bigger than 1. The inspiration behind $f_2(\rho)$ comes from the 1D function $f(x) = (\cos x + ia \sin x)^N$, whose supergrowing and imaging properties have been studied in

depth already [12, 15]. We choose $k_{f_2} \gg k_{f_1}$, where k_{f_1} is four times the full-width-half-maximum of the Fourier transform of $f_1(\rho)$. The bandlimit criterion is satisfied as $k_{f_2} + k_{f_1} = bk_{\max}^s$, where $0.75 \leq b \leq 0.95$. Then, $f(\rho)$ supergrows locally within the spatial limit when $a \gg 1$.

The ability of this analytical function to generate supergrowth is limited. Numerical simulations help us overcome this obstacle. To find the appropriate fields that supergrow within the frequency and space limit on the image plane Z_I , we perform simulations using the Zernike polynomial-Bessel function basis for circular symmetric functions, and simultaneously adopt the Helmholtz equation-based definition of local wavenumber/growth rate (Appendices E and F of Ref. [16]). A multi-objective cost optimization is performed to ensure 1) optimum extent of supergrowing region within the image plane, 2) optimization of the ratio of maximum intensity within the supergrowing region and the maximum intensity in the image plane. The second condition ensures the effect of enhanced sidelobes, a limitation observed in superoscillation-based superresolution imaging, is curtailed [7].

Supergrowing area Υ_s of measured image.— Supergrowing area denotes the fraction of the area of a complex field that is supergrowing at the image plane. Υ_s is another tool for quantifying the quality of the supergrowing field—a higher value of Υ_s is better. But this definition of Υ_s is inadequate for images obtained from the experiment due to noise. Let $f(x, y)$ be the complex field at the image plane (Fig. 2). In the experiment, the CCD measures the spatially discretized and noisy version of intensity $I(x, y) = |f(x, y)|^2$ as $I_0(m, n)$, where m, n are matrix indices of the matrix representing CCD pixels. We have ensured the maximum spatial frequency of the field is much smaller than the frequency of the CCD pix-

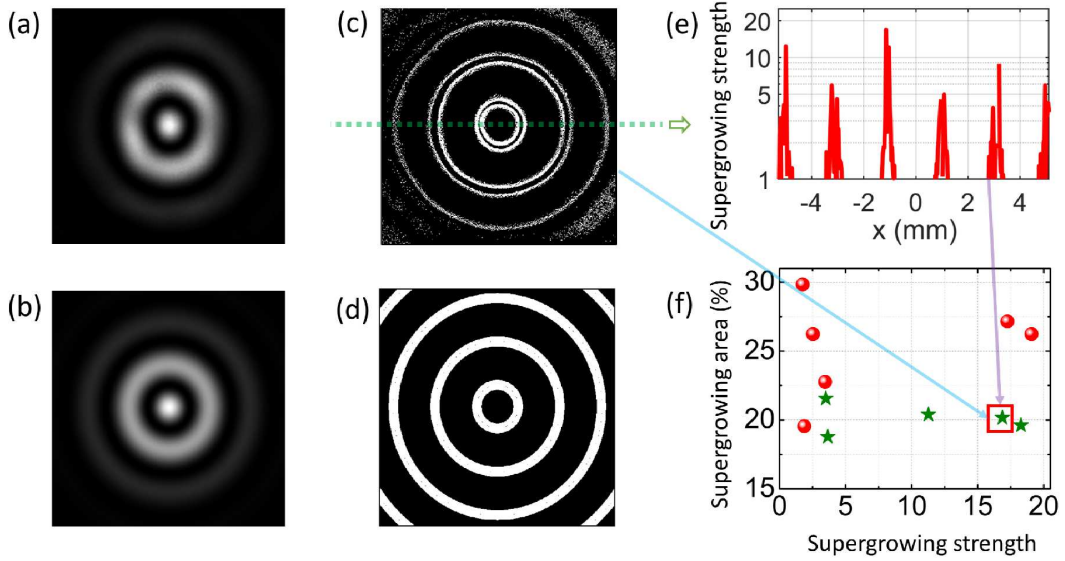


FIG. 4. Intensity of a synthesized field at the image plane z_I (Fig. 2), measured using the CCD, is shown in (a) and the corresponding analytical function is shown in (b). Panels (c) and (d) identify the supergrowing regions of measured and theoretical fields, respectively, in white. Supergrowing strength Γ_s of supergrowing regions identified in (c) along a horizontal line cut (highlighted using a semi-transparent dashed green line) is shown in (e). We have averaged four adjacent rows of pixels to get this line cut to reduce the effect of noise. Panel (f) shows the quality of supergrowth of multiple fields, synthesized in the experiment, represented here by plotting supergrowing area Υ_s and maximum supergrowing strength Γ_s along the x-linecut of each field. Here Red (green) spheres (stars) represent the function obtained using the simulations (heuristic method). The field shown in (a)-(e) is highlighted using a red square in (f). Simulations provide greater control over the supergrowing area of target fields, and corresponding experimental synthesis shows Υ_s between 19.5% and 29.8%.

els so that the Nyquist criterion is not violated. One can express $I_0(m, n) = \eta_d(m, n)I(m, n) + I_\xi(m, n)$, where, $\eta_d(m, n)$ is the detection efficiency of the pixel (m, n) , $I_\xi(m, n)$ is the noise, and $I(m, n)$ is discretized $I(x, y)$. The intensity quantization at each pixel is ignored in this representation.

Let the maximum value of the noise $I_\xi(m, n)$ be $I_{\xi 0}$. One cannot consider pixels with intensities $I_0(m, n) \leq I_{\xi 0}$. The supergrowing area of measured images can be defined as

$$\Upsilon_s = \frac{\zeta_s}{\zeta}, \quad (3)$$

where ζ is the total number of pixels with $I_0(m, n) \geq I_{\xi 0}$, and ζ_s is the total number of pixels with $\Gamma_s(m, n) \geq 1$ and $I_0(m, n) \geq I_{\xi 0}$.

Results.— We have prepared multiple bandlimited complex functions with finite spatial extent using analytical expression and simulation. The fields realized in the experiment have a diverse range of supergrowing strength Γ_s and area Υ_s . Figure 3 demonstrates the ability to control the supergrowth of the synthesized field (with respect to k_{\max}^s) in the experiment. Row (1) of the figure shows a field with maximum $\Gamma_s \approx 40$ (≈ 18.3 , in the experiment), while the field shown in row (2) is not supergrowing ($\Gamma_s < 1$).

A transverse distribution of intensity and corresponding supergrowing regions at the image plane Z_I [Fig. 2] of a representative complex field (both in theory and experiment) are demonstrated in Figs. 4(a)-(d). The supergrowing area of this field is $\Upsilon_s \approx 23.6\%$ ($\approx 20.16\%$, in the experiment). The experiment exhibits lower Υ_s and double-ring patterns [Fig. 4(c)] because pixels with intensities less than the cutoff $I_{\xi 0}$ [Eq. (3)] are ignored. Note, for such 2D images of intensity $I(x, y)$, we calculate the local intensity growth rate as $\kappa_I(x, y) = |\nabla \log [I(x, y)]|$. By definition, supergrowth is more sensitive to fluctuations at low intensities. In the experiment, noise/distortions present at intensities comparable to the noise floor can lead to identifying more supergrowing regions than the analytical field. The definition of Υ_s [Eq. (3)] reduces this effect by neglecting low-intensity pixels.

Measured values of the supergrowing area Υ_s and the maximum values of supergrowing strength Γ_s for multiple supergrowing fields synthesized in the experiment are shown in Fig. 4(f). One can observe that the functions obtained from the simulations, in general, can attain larger values of Υ_s . This is consistent with the multiobjective optimization conditions described previously. We have achieved a significantly larger supergrowing area (up to $\Upsilon_s \approx 29.8\%$) as well as a maximum local growth rate reaching up to ≈ 19.1 times of the bandlimit of the

system. A supergrowing strength of ~ 19 is highly desirable since optical spots with high local growth rates help us image subwavelength objects.

Discussion.— We have demonstrated the experimental synthesis of supergrowing optical fields. We also prescribe comprehensive methods and parameters to measure and characterize the supergrowth in an experiment. In this context, we have clarified the distinction between the supergrowth of an optical field and the concept of supergrowth in a diffraction-limited optical system. While the latter provides a stronger constraint on the condition of supergrowth, we are still able to achieve local growth rates more than an order of magnitude higher in our setup compared to the system bandlimit. Additionally, our setup shows excellent control over supergrowth since we realize optical fields with a diverse range of supergrowing areas and strengths. Supergrowing regions inherently can contain exponentially higher intensities compared to superoscillating regions [12, 15]. Therefore, supergrowth will alleviate the effect of enhanced sidelobes plaguing superoscillation-based imaging and improve SNR in experiments. This letter lays the groundwork for generating supergrowth in the lab and serves as the foundation for a novel superresolution imaging system.

A natural next step is to realize supergrowth-based subwavelength object reconstruction proposed in Ref. [15]. Also, supergrowth being a weak value amplification of momentum [11], generating optical fields with higher supergrowing strengths could be useful in a multitude of applications as well, including communication and quantum technologies. Furthermore, an optical field spot with simultaneously optimized supergrowing and superoscillating properties could prove to be extremely beneficial for superresolution imaging.

We acknowledge insights provided by Abhishek Chakraborty, Arunabh Mukherjee, and Valeria Viteri-Pflucker in this project. This work was supported by the AFOSR grant #FA9550-21-1-0322 and the Bill Hannon Foundation.

* skarimpa@ur.rochester.edu

† tkarmaka@ur.rochester.edu

‡ nick.vamivakas@rochester.edu

- [1] J. W. Goodman, *Introduction to Fourier Optics*, fourth edition ed. (W.H. Freeman, Macmillan Learning, New York, 2017).
- [2] Y. Aharonov, S. Popescu, and D. Rohrlich, How can an

infra-red photon behave as a gamma ray?, Tel-Aviv University Preprint TAUP **1847–90**.

- [3] G. Chen, Z.-Q. Wen, and C.-W. Qiu, Superoscillation: from physics to optical applications, *Light: Science & Applications* **8**, 56 (2019).
- [4] G. Gbur, Using superoscillations for superresolved imaging and subwavelength focusing, *Nanophotonics* **8**, 205 (2019).
- [5] M. V. Berry and S. Popescu, Evolution of quantum superoscillations and optical superresolution without evanescent waves, *J. Phys. A: Math. Gen.* **39**, 6965 (2006).
- [6] M. Berry, N. Zheludev, Y. Aharonov, F. Colombo, I. Sabadini, D. C. Struppa, J. Tollaksen, E. T. Rogers, F. Qin, M. Hong, *et al.*, Roadmap on superoscillations, *Journal of Optics* **21**, 053002 (2019).
- [7] K. S. Rogers, K. N. Bourdakos, G. H. Yuan, S. Mahajan, and E. T. F. Rogers, Optimising superoscillatory spots for far-field super-resolution imaging, *Optics Express* **26**, 8095 (2018).
- [8] Y. Hu, S. Wang, J. Jia, S. Fu, H. Yin, Z. Li, and Z. Chen, Optical superoscillatory waves without side lobes along a symmetric cut, *Advanced Photonics* **3**, 045002 (2021).
- [9] Y. Kozawa, D. Matsunaga, and S. Sato, Superresolution imaging via superoscillation focusing of a radially polarized beam, *Optica* **5**, 86 (2018).
- [10] X. H. Dong, A. M. H. Wong, M. Kim, and G. V. Eleftheriades, Superresolution far-field imaging of complex objects using reduced superoscillating ripples, *Optica* **4**, 1126 (2017).
- [11] A. N. Jordan, Y. Aharonov, D. C. Struppa, F. Colombo, I. Sabadini, T. Shushi, J. Tollaksen, J. C. Howell, and A. N. Vamivakas, Superphenomena in arbitrary quantum observables (2022), [arXiv:2209.05650](https://arxiv.org/abs/2209.05650) [math-ph, physics:quant-ph].
- [12] A. N. Jordan, Superresolution using supergrowth and intensity contrast imaging, *Quantum Studies: Mathematics and Foundations* **7**, 285 (2020).
- [13] D. W. Pohl, W. Denk, and M. Lanz, Optical stethoscopy: Image recording with resolution $\lambda/20$, *Applied Physics Letters* **44**, 651 (1984).
- [14] H. Yang, N. Moullan, J. Auwerx, and M. A. M. Gijs, Super-Resolution Biological Microscopy Using Virtual Imaging by a Microsphere Nanoscope, *Small* **10**, 1712 (2014).
- [15] T. Karmakar, A. Chakraborty, A. N. Vamivakas, and A. N. Jordan, Supergrowth and sub-wavelength object imaging (2023), [arXiv:2307.03352](https://arxiv.org/abs/2307.03352) [physics.optics].
- [16] T. Karmakar and A. N. Jordan, Beyond superoscillation: General theory of approximation with bandlimited functions (2023), [arXiv:2306.03963](https://arxiv.org/abs/2306.03963) [math-ph].
- [17] V. Arrizón, U. Ruiz, R. Carrada, and L. A. González, Pixelated phase computer holograms for the accurate encoding of scalar complex fields, *J. Opt. Soc. Am. A* **24**, 3500 (2007).